LAWRENCE
LIVERMORE
NATIONAL
LABORATORY

LLNL-CONF-425427

# Mesoscale Modeling of LX-17 Under Isentropic Compression

H. K. Springer, T. M. Willey, G. Friedman, L. E. Fried, K. S. Vandersall, M. R. Baer

March 12, 2010

14th International Detonation Symposium
Coeur d'Alene, ID, United States
April 11, 2010 through April 16, 2010

## Disclaimer

# Mesoscale Modeling of LX-17 Under Isentropic Compression

H. Keo Springer*, Trevor M. Willey*, Gary Friedman*, Laurence E. Fried*, Kevin S. Vandersall*, Melvin R. Baer**

*Lawrence Livermore National Laboratory, Livermore, CA 94551

**Sandia National Laboratory, Albuquerque, NM 87185

**Abstract.** Mesoscale simulations of LX-17 incorporating different equilibrium mixture models were used to investigate the unreacted equation-of-state (UEOS) of TATB. Candidate TATB UEOS were calculated using the equilibrium mixture models and benchmarked with mesoscale simulations of isentropic compression experiments (ICE). X-ray computed tomography (XRCT) data provided the basis for initializing the simulations with realistic microstructural details. Three equilibrium mixture models were used in this study. The single constituent with conservation equations (SCCE) model was based on a mass-fraction weighted specific volume and the conservation of mass, momentum, and energy. The single constituent equation-of-state (SCEOS) model was based on a mass-fraction weighted specific volume and the equation-of-state of the constituents. The kinetic energy averaging (KEA) model was based on a mass-fraction weighted particle velocity mixture rule and the conservation equations. The SCEOS model yielded the stiffest TATB EOS ($0.121\mu + 0.4958\mu^2 + 2.0473\mu^3$) and, when incorporated in mesoscale simulations of the ICE, demonstrated the best agreement with VISAR velocity data for both specimen thicknesses. The SCCE model yielded a relatively more compliant EOS ($0.1999\mu - 0.6967\mu^2 + 4.9546\mu^3$) and the KEA model yielded the most compliant EOS ($0.2105\mu - 1.2618\mu^2 + 5.9912\mu^3$) of all the equilibrium mixture models. Mesoscale simulations with the lower density TATB adiabatic EOS data demonstrated the least agreement with VISAR velocity data.

## Introduction

The quasi-isentropic compression experiments (ICE) on Sandia National Laboratory's Z-Accelerator have been extensively used for determining the unreacted equation-of-state (UEOS) of explosives because it is able to attain high pressures without significant reaction or detonation [1-7]. While continuum-scale studies have previously investigated LX-17 (92.5% TATB, 7.5% Kel-F 800) under isentropic compression loading [5], there have been fewer studies focused on TATB constituent response in these explosive mixtures. Moreover, existing TATB shock data [8] based on adiabatic shock conditions is not necessarily relevant to these loading conditions.

The primary objective of this study is to determine a TATB UEOS using equilibrium mixture models and mesoscale simulations. Equilibrium mixture models provide a method for predicting the UEOS of energetic material grains

in an explosive mixture, given sufficient information of the overall mixture and binder phase [9-11]. Since Kel-F 800 [12] and LX-17 [5] have been adequately characterized in previous ICE, we will use the equilibrium mixture models to develop candidate TATB UEOS. Mesoscale simulations of the LX-17 ICE will then be used to benchmark the performance of the different equilibrium mixture models. We will initialize the mesoscale simulations with realistic microstructure data in order to capture the interactions between the heterogeneous TATB and Kel-F 800 phases, as part of developing an accurate framework for validating candidate TATB UEOS.

**Description of Mesoscale Simulations**

Three-dimensional mesoscale simulations of the LX-17 ICE were performed using LLNL's multi-physics, arbitrary-lagrangian-eulerian code, ALE3D [13]. The LX-17 ICE geometry consisted of a 400 μm aluminum substrate underlying 0.6 cm diameter and 300 or 350 μm thick LX-17 specimens. A LiF optical window was bonded to the back of the LX-17 specimens, minimizing wave reflections while enabling the interface velocity to be tracked with single-point VISAR. The applied pressure pulse had been previously derived from the experimental current (B-dot) measurements and is shown in Figure 1 [5]. The pressure pulse consists of a pressure up to 0.175 Mbar with a rise-time of 0.3 μs and is applied to the aluminum substrate in the simulations.

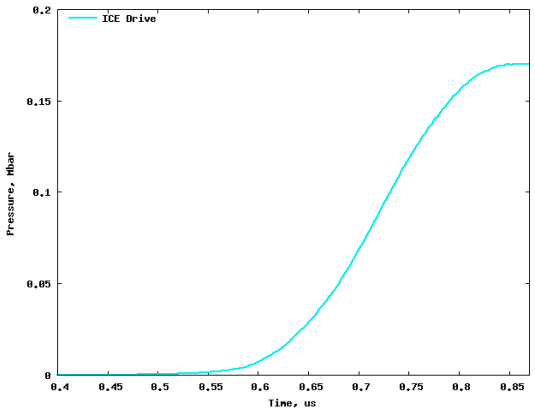

Fig. 1. Isentropic compression drive.

The UEOS parameters used in these simulations for aluminum [14], LiF [14], Kel-F 800 [12], and TATB [8] are shown in Table 1. Based on Reisman et al. [5], we used a Jones-Wilkins-Lee (JWL) model for the LX-17 UEOS:

$$P = Ae^{-R_1 v_r} + Be^{-R_2 v_r} + \frac{\omega C_V T}{v_r} \qquad (1)$$

where $P$ is the pressure, $T$ is the temperature, and $v_r$ is the relative volume (ratio of current-to-initial specific volume $= \frac{v}{v_0}$). For LX-17, the density is 1.90 g/cc, $A$ is 778.1 Mbar, $B$ is -0.05031 Mbar, $R_1$ is 11.3 , $R_2$ is 1.13 , and $\omega$ is 0.8938. No strength models were used in these simulations.

Table 1. Material EOS parameters.

| **Material** | $\rho_0$ **(g/cc)** | $c$ **(cm/μs)** | $S_1$ | $\Gamma_0$ |
|---|---|---|---|---|
| Kel-F 800 [12] | 2.017 | 0.1745 | 1.993 | 1.097 |
| Aluminum 6061-T6 [14] | 2.703 | 0.524 | 1.40 | 1.97 |
| LiF [14] | 2.638 | 0.515 | 1.35 | 1.69 |
| TATB [8] | 1.847 | 0.234 | 2.316 | 1.6 |
| TATB [8] | 1.937 | 0.29 | 1.68 | 0.2 |

X-ray Computed Tomography (XRCT) Initialization

We initialized the mesoscale simulations with LX-17 microstructure data from x-ray computed tomography (XRCT) studies. The realistic microstructure enabled our simulations to better capture the interactions between TATB and Kel-F 800 phases, as we evaluated the equilibrium mixture models. Figure 2 shows the density fringe plot of the volumetric XRCT data-set, which is approximately 0.3 cm x 0.3 cm x 0.3 cm with a resolution of 17 μm. The prill boundaries are distinguished by the red zones in this plot.

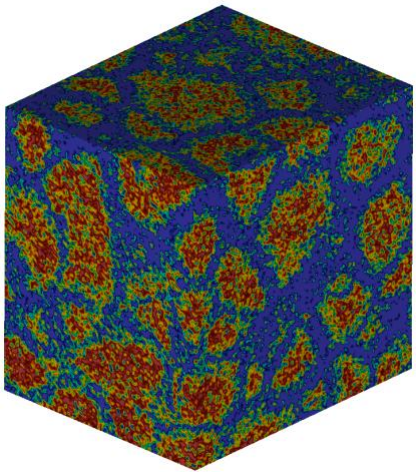

Fig. 2. Density fringe plot of the XRCT data-set. The overall size of domain is 0.3 cm x 0.3 cm x 0.3 cm with a voxel/element resolution of 17 μm.

The synchrotron based tomography data were acquired at beamline 8.3.2 at the Advanced Light Source, Lawrence Berkeley National Laboratory [15], using a photon energy of 20 keV. X-rays of 25 and 30 keV were also used to determine composition. Every 20 views, bright field images were acquired to normalize incident x-ray flux and the decay in the synchrotron storage ring source current; dark field images were also acquired. The transmitted x-rays impinge upon a $CdWO_4$ single crystal scintillator, and are recorded by a Cooke PCO 4000 CCD camera. In order to minimize phase effects, the camera and scintillator box are moved as close as possible to the specimen.

Tomographic slices were reconstructed via filtered back projection using the LLNL-developed ImageRec code to retrieve linear attenuation coefficients for each voxel within the volume. In order to remove ring artifacts from each sinogram, each row was fit with the attenuation expected from a cylinder, and the rows and fits were averaged. This allowed for deconvolution of the x-ray attenuation through the part from artifacts introduced by the detector, scintillator, camera optics, and by inhomogeneous x-ray illumination.

Multiple datasets acquired at different monochromatic photon energies can be used to quantitatively determine constituent volume fractions, voxel by voxel, in a three dimensional volume[16-17]. Quantitative CT reconstructions return linear attenuation coefficients[18] for each voxel. For this particular volume used, we calibrated a single acquisition to a previous study[16-17] and derived constituent volume fractions. An algorithm was developed to import this data into an ALE3D model mesh while maintaining the same dimensional and constituent volume fractions.

**Equilibrium Mixture Models**

We calculated candidate TATB UEOS using equilibrium mixture models and benchmarked these models with mesoscale simulations of ICE. Three equilibrium mixture models were used in this study: single constituent with conservation equations (SCCE) model, single constituent equation-of-state (SCEOS) model, and the kinetic energy averaging (KEA) model [19]. The TATB UEOS derived from these equilibrium mixture models were compared to existing TATB data, both in p-μ space and as it compares directly to VISAR data.

Fundamental to the SCCE and SCEOS models was the mass-fraction weighted specific volume mixture rule and the enforcement of pressure-equilibrium. We used a mass-fraction weighted specific volume for a two-phase system that can be written as:

$$\bar{v}\ (P,T) = x_1 v_1\ (P,T) + x_2 v_2\ (P,T)$$
$$v_1\ (P,T) = \frac{\bar{v}\ (P,T) - x_2 v_2\ (P,T)}{x_1} \qquad (2)$$

where $\bar{v}$ is the specific volume of the mixture, and $v_i, x_i$ are the specific volumes and mass fractions of the *ith* phase. For LX-17, the mass fraction of TATB ($x_1$) is 0.925 and Kel-F 800 ($x_2$) is 0.075. The specific volume mixture rule yields an initial TATB density of 1.891 g/cc.

The secant method was used to determine the (roots) specific volumes of LX-17 and Kel-F 800 used in (2), while enforcing pressure-equilibrium at incrementally higher pressures. This information was used to create the $P-v$ curve and UEOS in a

linear polynomial form written as:

$$P = a_1\mu + a_2\mu^2 + a_3\mu^3 \qquad (3)$$

where $a_i$ are the coefficients of the linear polynomial form and $\mu$ is a volumetric parameter related to the specific volume by $\mu = \frac{v_0 - v}{v}$.

SCCE Model

The SCCE model employs the governing conservation equations in (4) and enforces pressure-equilibrium for each LX-17 and Kel-F 800 to determine the specific volumes at discrete pressure values. The $P - v$ response of TATB is then determined using (2). The governing mass, momentum, and energy conservation equations in Eulerian form for a one-dimensional shock wave are:

$$\begin{aligned} &\frac{\partial \rho}{\partial t} + \nabla\ \rho u\ = 0 \\ &\frac{\partial\ \rho u}{\partial t} + \nabla\ \rho u^2 + P\ = 0 \\ &\frac{\partial\ \rho e}{\partial t} + \nabla u\left(\rho e + \frac{1}{2}\rho u^2 + P\right) = 0 \end{aligned} \qquad (4)$$

where $\rho$ is the density, $u$ is the material velocity, and $e$ is the specific internal energy. These can be simplified for the case of a steady shock wave:

$$\begin{aligned} &\rho_0 U = \rho\ U - u \\ &P = \rho_0 U u \\ &e - e_0 = \frac{1}{2}u^2 \end{aligned} \qquad (5)$$

where $U$ is the steady shock velocity, and $e_0$ is the initial specific internal energy. Given a $U - u$ relationship for LX-17 and Kel-F 800 (Table 1) and increasing pressure values, we determine the particle velocity in (5b), density in (5a), and energy in (5c).

The resulting TATB UEOS linear polynomial parameterization is shown in Table 2 and a comparison is made to the SCEOS and KEA models, as well as LX-17, Kel-F 800, and existing TATB data, in Figure 3. The parameters for linear polynomial form EOS are as follows: $0.1999\mu - 0.6967\mu^2 + 4.9546\mu^3$.

Applying the conservation equations to each constituent separately assumes that no momentum or energy is transferred during loading. The accuracy of this assumption is not well known considering the heterogeneous nature of this microstructure and the impulsive loading.

Table 2. TATB UEOS linear polynomial parameters based on equilibrium mixture models.

| **Model** | $a_1$ **(Mbar)** | $a_2$ **(Mbar)** | $a_3$ **(Mbar)** |
|---|---|---|---|
| SCCE | 0.1999 | -0.6967 | 4.9546 |
| SCEOS | 0.121 | 0.4958 | 2.0473 |
| KEA | 0.2105 | -1.2618 | 5.9912 |

SCEOS Model

The SCEOS model employs the equation-of-state in (1) and enforces pressure-equilibrium for each LX-17 and Kel-F 800 to determine $\mu$, thus $v$, at increasing pressure values. The $P - v$ response of TATB is then determined using (2). The resulting TATB UEOS linear polynomial parameterization is shown in Table 2 and a comparison is made to other models and data in Figure 3. The parameters for linear polynomial form EOS are as follows: $0.121\mu + 0.4958\mu^2 + 2.0473\mu^3$. As shown in Figure 3, the SCEOS model yielded the stiffest EOS for TATB, as compared with the SCCE and KEA models.

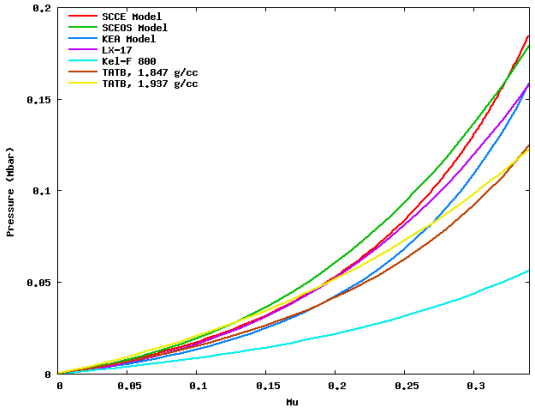


Fig. 3. A comparison of the equilibrium mixture models in $P-\mu$ space with the experimental TATB, LX-17, and Kel-F 800 data.

KEA Model

The KEA model employs a mass-fraction weighted particle velocity averaging relationship shown in (6). This model is based on the work of Batsanov [19] and was demonstrated to accurately predict EOS mixtures [11]. Pressure-equilibrium is enforced on (5c) for each LX-17 and Kel-F 800 to determine particle velocity at increasingly higher pressures for substitution in (6). The particle velocity is related to the volumetric parameter in (5a) to develop a $P-\mu$ curve. The particle velocity averaging relationship is written as:

$$\bar{u}^2 = x_1 u_1^2 + x_2 u_2^2$$
$$u_1 = \left[ \frac{\bar{u}^2 - x_2 u_2^2}{x_1} \right] \qquad (6)$$

where $\bar{u}$ is the particle velocity of LX-17, $u_1, x_1$ is the particle velocity and mass fraction of the TATB and $u_2, x_2$ is the particle velocity and mass fraction of the Kel-F 800. The resulting TATB UEOS linear polynomial parameterization is shown in Table 2 and a comparison is made to other models and data in Figure 3. The parameters for linear polynomial form EOS are as follows: $0.2105\mu - 1.2618\mu^2 + 5.9912\mu^3$. As shown in Figure 3, the KEA model yielded the most compliant EOS of all the equilibrium mixture models, as compared with the SCCE and the SCEOS models.

**Results of Mesoscale Simulations of LX-17 ICE**

Figure 4 shows the progression of a mesoscale simulation of LX-17 ICE (350 μm thick). LX-17 microstructural initialization is shown by virtue of a density fringe plot. The pressure impulse is shown propagating from the free surface of the aluminum substrate to the LX-17 specimen and then the LiF optical window. The velocity of the specimen-window interface is used as a metric of the specimen EOS.

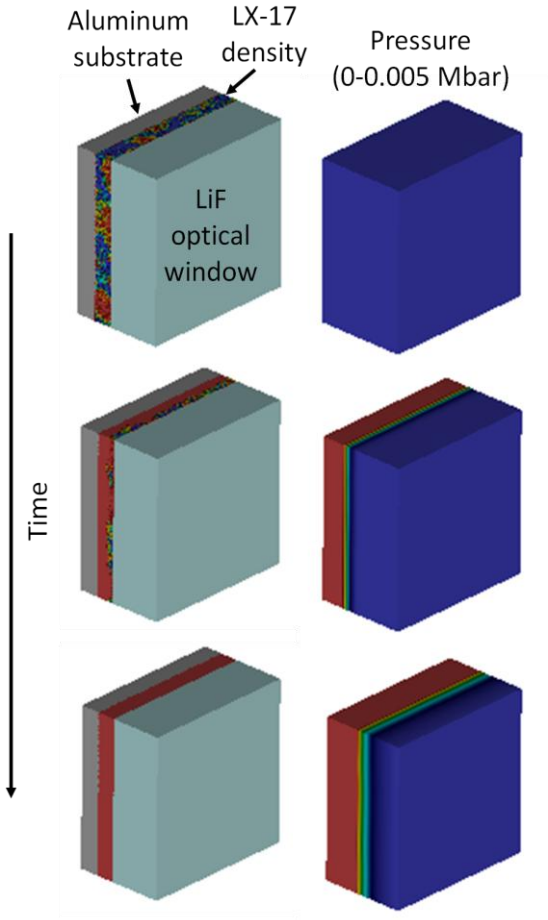


Figure 4: Progression of a mesoscale simulation of the ICE. Density fringe plot is shown for the LX-17 on the left. The scale for the pressure fringe plot on the right is 0-0.005 Mbar.

Figures 5 and 6 show plots of the specimen-window interface velocity predicted by the mesoscale simulations and the VISAR measurements for the 300 and 350 μm thick LX-17 specimens. Predictions are made incorporating the SCCE, SCEOS, and KEA models, as well as the 1.847 g/cc and 1.937 g/cc TATB shock data. The delay in the onset of interface motion measured by VISAR is due to the transit time through the aluminum substrate and the thinner (earlier onset) or thicker (later onset) specimens.

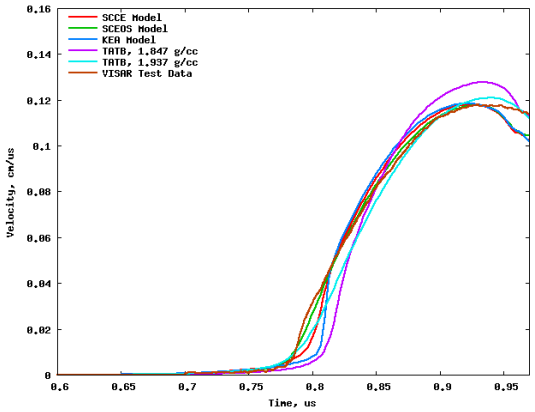


Figure 5: Equilibrium mixture model predictions and TATB data based predictions compared with VISAR velocity data for the 300 μm thick LX-17 specimens. The SCEOS model predictions demonstrate the best agreement with experimental data.

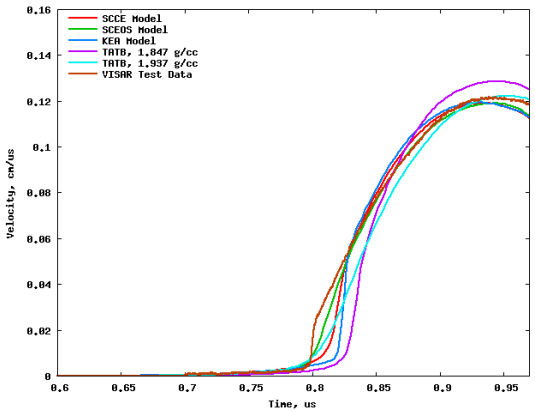


Figure 6: Equilibrium mixture model predictions and TATB data based predictions compared with VISAR velocity data for the 350 μm thick LX-17 specimens. The SCEOS model predictions demonstrate the best agreement with experimental data.

Simulation predictions based on the SCEOS model demonstrated the best agreement with the VISAR measurements during interface acceleration (i.e., onset of motion to peak velocity) for both specimen thicknesses. For the SCEOS model, better agreement is observed for the thinner specimens than for thicker specimens during the initial interface acceleration (up to 0.05 cm/μs). During the interface deceleration (i.e., post-peak velocity and unloading), it is uncertain whether the specimen-window interface is intact and, therefore, this VISAR data is not considered in comparisons with the models.

Simulation predictions based on the SCCE model demonstrated better agreement with the VISAR measurements than the KEA model during interface acceleration for both specimen thicknesses. For each the SCCE and the KEA models, better agreement is observed for the thinner specimens than for thicker specimens. An appreciable delay is observed during initial interface acceleration for both models compared with the SCEOS model. This delay is a result of the relatively higher EOS stiffness associated with the SCEOS model as shown in Figure 3.

Simulation predictions based on the high density (1.937 g/cc) TATB data demonstrated better agreement to the VISAR measurements than the low density (1.847 g/cc) TATB data. The low density TATB demonstrated the least overall agreement with the VISAR measurements. A smaller delay during initial acceleration and better tracking with VISAR measurements was observed for the higher density TATB. For each the higher and lower density TATB, better agreement is observed for the thinner specimens than for thicker specimens.

## Conclusions

Benchmarking the candidate TATB UEOS from the equilibrium mixture models with the 3D mesoscale simulations of ICE, we found that the SCEOS model demonstrated the best agreement with VISAR measurements. Considering the Figure 3 EOS comparison of LX-17 (more stiff

EOS than Kel-F 800) and Kel-F 800 (more compliant EOS than LX-17), we would expect that the model yielding an EOS stiffer than LX-17 is necessary to produce better agreement with the test data. In fact, the SCEOS and SCCE models are the only two models that fall in this category. So, EOS data plots of the constituents and the mixture then serve as a screening tool for efficacy of the model even before mesoscale simulations. Altogether, we demonstrated that the pressure-equilbrium with constituent EOS and mass-fraction specific volume mixture rule are sufficient to get the energetic grain EOS in an explosive mixture. In the future, this should be attempted for other TATB-based explosive mixture (e.g., PBX-9502) and other explosive types with significantly different grain volume fractions and size distributions. Future equilibrium mixture models may need to contain details on the grain volume fraction and size distribution to be applicable over many different types of explosives.

Overall, we validated the modeling approach of using mesoscale simulations initialized with detailed LX-17 microstructure from XRCT to capture the average interface velocity. In the future, it is also desirable to compare predictions of the spatially-fluctuating field with line VISAR or similar techniques. This data could be used to validate future equilibrium mixture models incorporating microstructural details.

**Acknowledgements**

We wish to acknowledge the assistance of D. B. Reisman with reviewing previous LX-17 ICE studies, as well as S. Bastea and P. Sterne for helpful discussions on the equilibrium mixture models. This work performed under the auspices of the U.S. Department of Energy by Lawrence Livermore National Laboratory under Contract DE-AC52-07NA27344.

## References

1. Hall, C.A., "Isentropic Compression Experiments on the Sandia Z Accelerator," *Phys. Plasmas* 7, pp. 2069, 2000.

2. Hall, C.A., Asay, J. R., Knudson, M. D., Stygar, W. A., Spielman, R. B., Pointon, T. D., Reisman, D., Toor, A., and Cauble, R. C., *Rev. Sci. Instrum.* Vol. 72, pp. 3587, 2001.

3. Reisman, D. B., *et al.*, "Isentropic Compression of LX-04 on the Z accelerator" in *Shock Compression of Condensed Matter*, edited by Furnish, M. D., Thadhani, N. N., and Horie, Y., AIP Press, Melville, NY, pp. 849–852, 2001.

4. Reisman, D. B., Toor, A., Cauble, R. C., Hill, C. A., Asay, J. R., Knudson, M. D., and Furnish, M. D., "Magnetically driven isentropic compression experiments on the Z-accelerator," *J. Appl. Phys.* Vol. 89, pp. 1625, 2001.

5. Reisman, D. B., Forbes, J., Tarver, C., Garcia, F., Hayes, D., Furnish, M., and Dick, J., "Isentropic Compression of High Explosives with the Z Accelerator," *Proceedings of the 12th International Detonation Symposium*, pp. 343-348, San Diego, CA, August 2002.

6. Hare, D. E., Reisman, D. B., Garcia, F., Green, L. G., Forbes, J. W., Furnish, M. D., Hall, C. A., and Hickman, R. J., *Shock Compression of Condensed Matter*, edited by M. D. Furnish, Y. M. Gupta, and J. W. Forbes, AIP Press, Melville, NY, 2003, pp. 145–148.

7. Vandersall, K.S., Reisman, D. B., Forbes, J. W., Hare, D. E., Garcia, F., Uphaus, T. M., Elsholz, A. J., Tarver, C. M., and Eggert, J. H., "Isentropic Compression Experiments Performed By LLNL On Energetic Material Samples Using The Z-Accelerator", *LLNL Report, UCRL-TR-236063*, 2007.

8. Dobratz, B. and Crawford, P., "LLNL Explosives Handbook", *LLNL Report UCRL-52997 Change 2*, 1985.

9. Krueger, B.R., Vreeland, T., "A Hugoniot theory for solid and powder mixtures", *J. Appl. Phys.*, Vol. 69:2, pp. 710–716, 1991.

10. Saurel, R., Le Metayer, O., Massoni, J., Gavrilyuk, S., "Shock jump relations for multiphase mixtures with stiff mechanical relaxation", *Shock Waves*, Vol. 16:3, pp. 209–232, 2007.

11. Petel, O., Jette, F., "Comparison of Methods for Calculating the Shock Hugoniot of Mixtures", *Shock Waves*, Vol. 20, pp. 73-83, 2010.

12. Clements, B., Mariucescu, L., Brown, E., Rae, P., Orler, E., Dattelbaum, D., Sheffield, S., Robbins, D., Gustavsen, R., and Velisavljevic, N., "Kel-F 800 Experimental Characterization and Model Development", *Los Alamos National Laboratory Report LA-UR-07-6404*, 2007.

13. Nichols, A., “Users Manual for ALE3D: An Arbitrary Lagrange/Eulerian 3D Code System”, *Lawrence Livermore National Laboratory Report UCRL-MA-152204 Rev 6*, 2007.
14. Steinberg, D. J., “Equation of state and strength properties of selected materials” *LLNL Report UCRL-MA-106439*, 1996.
15. Robin, D., Krupnick, J., Schlueter R., Steier, C., Marks, S., et al., "Superbend upgrade on the Advanced Light Source", *Nuclear Instruments & Methods in Physics Research Section a-Accelerators Spectrometers Detectors and Associated Equipment*, Vol. 538, pp. 65-92, 2005.
16. Kinney, J.H., Willey, T.M., and Overturf, G.E., "On the Nature of Variations in Density and Composition within TATB-based Plastic Bonded Explosives", *Proceedings of the 13th International Detonation Symposium*. pp. 388-392, Norfolk, VA, USA, July 23-28, 2006.
17. Willey, T.M. and Overturf, G.E., "Towards Next Generation TATB-based Explosives by Understanding Voids and Microstructure from 10 nm to 1 cm", *Proceedings of the 40th International Conference of the Fraunhofer Institute for Chemical Technology: Energetic Materials: Characterization Modelling, and Validation*. pp. V19.1-V19.12, Karlsruhe, Germany, June 23-29, 2009.
18. Henke, B.L., Gullikson, E.M., and Davis, J.C., "X-Ray Interactions - Photoabsorption, Scattering, Transmission, and Reflection at E=50-30,000 Ev, Z=1-92", *Atomic Data and Nuclear Data Tables*, Vol. 54, pp. 181-342, 1993.
19. Batsanov, S.S., “Effects of explosions on materials: modification and synthesis under high-pressure shock compression”. Springer, Berlin, 1994.